JBMR Plus, 2025, **9**, ziaf016
https://doi.org/10.1093/jbmrpl/ziaf016
Advance access publication: January 27, 2025
Research Article

Endplate remodeling: a key indicator of cigarette smoke exposure–induced intervertebral disc degeneration in a male rat model

Joshua Kelley[1], Hui Li[1], Yi Sun[2], Pengling Ren[3], Guanghua Chen[2], Shuchun Sun[1], Jichao Zhao[1], Nathan Buchweitz[1], Michael Kern[4], Charles A. Reitman[5], Danyelle M. Townsend[6], Hai Yao[1,7], Yongren Wu[1,5,*]

[1]Department of Bioengineering, Clemson University, 29425 Charleston, SC, United States
[2]Department of Orthopedics, The 2nd Affiliated Hospital of Harbin Medical University, 150086 Harbin, China
[3]Department of Radiology, Beijing Friendship Hospital, Capital Medical University, 100050 Beijing, China
[4]Department of Regenerative Medicine & Cell Biology, Medical University of South Carolina, 29425 Charleston, SC, United States
[5]Department of Orthopaedics and Physical Medicine, Medical University of South Carolina, 29425 Charleston, SC, United States
[6]Department of Drug Discovery and Biomedical Sciences, Medical University of South Carolina, 29425 Charleston, SC, United States
[7]Department of Oral Health Sciences, Medical University of South Carolina, 29425 Charleston, SC, United States

*Corresponding author: Yongren Wu, Clemson-MUSC Bioengineering Program, Department of Bioengineering, Clemson University, 68 President Street, BE101D-MSC501, Charleston, SC 29425, United States (yongren@clemson.edu).

Abstract

Recent clinical studies have established a strong association between cigarette smoking and degenerative disc disease. Both in vitro and in vivo research indicated that cigarette smoke disrupts cellular homeostasis in the intervertebral disc (IVD), leading to spatiotemporal remodeling of the extracellular matrix, with a notable reduction in solute diffusivity within the cartilage endplate (CEP). As the CEP serves as a critical mechanical barrier and solute diffusion pathway for the IVD, both roles can be compromised by pathological changes in the tissue. This underscores the need for a more comprehensive examination of endplate remodeling during IVD degeneration, particularly in the context of cigarette smoking and cessation. The objective of this study was to perform a quantitative analysis of the structure-material property relationship changes in the endplate at tissue and cellular levels to determine how endplate mineralization progresses during IVD degeneration in the context of cigarette smoke exposure and cessation, using our previously developed Sprague-Dawley rat model. Our results indicate that cigarette smoke exposure–induced endplate remodeling is characterized by a higher CEP histological grade, increased aberrant CEP calcification level, and elevated bony endplate surface flatness score, all of which correlated with an accelerated chondrocyte cell life cycle. Smoke cessation alone was insufficient to reverse the mineralization progression in the endplate. Principal component analysis further identified alterations in endplate morphometry at the tissue level and disruptions in the chondrocyte life cycle at cellular level as key markers of degenerative remodeling. These findings establish endplate remodeling as a key indicator of smoke exposure–induced IVD degeneration and inform the development of novel therapeutic strategies aimed at preserving or improving disc health.

Keywords: aging, animal models, matrix mineralization, preclinical studies, disorders of calcium/phosphate metabolism, chondrocyte and cartilage biology

Lay Summary

Cigarette smoking is linked to the degeneration of intervertebral discs—the cushioning tissue between the bones of the spine. Rats were exposed to cigarette smoke in a chamber to mimic the effects of smoking. We investigated how smoke exposure and stopping exposure affected the disc's endplate, a crucial area for disc health. We found that smoke exposure caused significant damage to the endplate, including increased calcification (hardening) and flattening, and that stopping the smoke exposure did not reverse these changes. These findings highlight the lasting impact of smoking on spinal health and suggest potential targets for treating smoking-induced disc degeneration.

Introduction

The global prevalence of smoking has declined over the past 2 decades, from 32.7% in 2000 to 21.7% in 2020, yet cigarette smoking remains a pervasive habit with significant public health consequences.[1] While cigarette smoking is well-documented to correlate with various cancers, cardiovascular diseases, and chronic obstructive pulmonary disease,[2,3] recent clinical studies have increasingly highlighted its strong connection with certain orthopedic conditions,[4,5] particularly degenerative disc disease.[6–10] These studies have demonstrated that patients with a history of smoking are at increased risk for disc prolapse and herniation, reduced disc height, as well as development of subchondral Modic changes and endplate sclerosis, which contribute to impaired spinal stability and pain.[6–10]

Received: December 5, 2024. **Revised:** January 10, 2025. **Accepted:** January 14, 2025

Previous in vitro culture studies using nicotine or cigarette smoke extract have shown that toxic chemicals in cigarette smoke disrupt gene expression and cellular metabolism, impairing critical processes such as oxidative stress response, and the balance of extracellular matrix synthesis and degradation.[11–13] These disruptions compromise intervertebral disc (IVD) homeostasis, and, as confirmed by in vivo animal studies involving nicotine injection or cigarette smoke exposure, consequently drive degenerative remodeling within the IVD.[13,14] Notably, histological analysis revealed disorganization of the annulus fibrosis (AF) collagen fiber bundles, hyalinization and fibrosis of the nucleus pulposus (NP), and decreased NP cellularity.[13,15,16] Our previous study utilizing a Sprague-Dawley (SD) rat model provided a detailed understanding of the spatiotemporal IVD remodeling patterns induced by cigarette smoke exposure, through quantitative assessment of the 3-dimensional solute diffusion properties. Smoke exposure markedly reduced solute diffusivity and indicated the initiation of calcification, particularly in the cartilage endplate (CEP) region, as observed through multiphoton imaging.[14] Notably, smoking cessation alone was insufficient to reverse the adverse changes in solute diffusivity, with a continued decline in CEP porosity and further calcification, although the latter has not yet been systematically quantified.[14]

As previous studies have demonstrated, the endplate region, comprising both the CEP and bony endplate (BEP), plays a crucial role in IVD mechanics and nutrition.[17–19] Specifically, it helps minimize stress concentration at the disc-bone interface by acting as a transition layer between the softer disc tissue and the more rigid vertebral body.[20,21] Additionally, the endplate functions as a mechanical barrier to fluid convection, maintaining interstitial fluid pressurization within the disc, which enables it to better sustain compressive loads.[18,22] Furthermore, the endplate serves as a primary solute diffusion pathway for the IVD, facilitating solute exchange between the disc and the vascular network in the vertebral bone.[23,24] However, the endplate is particularly prone to mechanical failures under loading, leading to microfractures or detachment.[25,26] Pathological endplate changes, such as ossification and blood vessel invasion, have consistently been documented as concurrent evidence of IVD degeneration during the aging process.[27–30] These findings underscore the need for a more in-depth examination of the endplate remodeling in the context of cigarette smoking. Moreover, as smoking cessation becomes more widespread, it is essential to better understand how endplate remodeling processes during IVD degeneration to optimize post-cessation IVD health assessments and guide therapeutic intervention.

Based on observations of BEP vascular bud recession and reduced CEP diffusivity in previous smoke exposure and cessation animal studies,[15,30] we hypothesized that 2 mo of cigarette smoke exposure would lead to endplate pathological remodeling, characterized by elevated levels of CEP calcification spots, altered surface flatness of BEP, both of which are associated with an accelerated chondrocyte life cycle. Moreover, even after a 5-mo period of smoke cessation, endplate calcification severity is expected to progressively deteriorate, continuing to serve as a key predictor of IVD degeneration progression.[14] This study, using our previously developed SD rat smoke exposure model,[5] aimed to perform a quantitative analysis of the structure-material property relationship changes in the endplate at tissue and cellular levels to determine how endplate calcification and ossification progress during IVD degeneration process in the context of cigarette smoke exposure and cessation. Specifically, this study characterized endplate remodeling using histological staining, μ-CT, and surface flatness analysis. Moreover, alterations in the CEP chondrocyte life cycle were quantified by combining histological and immunofluorescent analyses. IVD degeneration was graded using a standardized histopathology scoring system for IVD degeneration in rat models. Additionally, the relationships between cell life cycle, endplate calcification and ossification, and IVD degeneration were characterized using statistical correlation and principal component analysis (PCA).

Materials and Methods

Study design

After receiving IACUC approval (protocol number: AR#3511) from the Medical University of South Carolina, 24 male pathogen-free 6-mo-old (skeletally mature[31]) SD rats (body mass: 419 ± 38 g; Envigo) were randomly assigned to 2 treatment cohorts: control ($n = 12$) and smoke exposure ($n = 12$). These rats were initially part of a femoral fracture healing study where, after 1 mo of smoke exposure, both femurs were broken in control and smoke exposure groups before completing another month of smoke exposure.[5] Sample size for that study was determined using an ANOVA power analysis with an alpha of .05, beta of .8, and moderate effect size of 0.3 (G*power for windows, Version 3.1.9.7).[5] Animals were individually housed in a helicobacter-free institutional facility with a 12-h light/dark cycle. Housing enclosures were free of contamination from smoke with adequate food (standard rodent chow; Teklad 2918, Envigo), tap water, and bedding (Teklad 1/8th inch, Envigo or ALPHA-Dri, Sinclair Coal & Oil). The smoke exposure cohort underwent daily cigarette smoke exposure, 2 h on weekdays and 1 h on weekends, for 2 mo in a custom-built smoke exposure apparatus, while the control cohort remained in their housing cages free of smoke (Figure S1A and B).[5,14] The smoke exposure dosage was controlled by monitoring total particulate matter (TPM; 198.3 ± 62.7 mg/m^3) using an exhaust membrane filter (Pallflex® EMFAB TX40H120-WW, Pall laboratories, Westborough, MA) downstream from the rat exposure chamber, simulating heavy smoking at approximately 1 pack of cigarettes per day.[5,14] Based on the comparison between rat and human musculoskeletal aging (ie, 1 rat month equals about 2.5 human years), 2 mo of smoke exposure followed by 5 mo of cessation in rats simulates approximately 5 yr of heavy smoking and 12.5 yr of cessation in humans.[32] To reduce irregularities in cigarette composition, research cigarettes (3R4F, University of Kentucky Tobacco Research & Development Center) were used for smoke exposure. Following 2 mo of cigarette smoke exposure, 6 rats from each cohort were randomly selected and euthanized with isoflurane (PHR2874, Sigma-Aldrich). The remaining rats were then subjected to a 5-mo smoke cessation period before also being euthanized using isoflurane. This procedure resulted in 4 experimental groups ($n = 6$ per group): control (2 mo without smoke exposure), smoke exposure (2 mo of smoke exposure), cessation control (7 mo without smoke exposure), and smoke cessation (2 mo with then 5 mo without smoke exposure; Figure S1C).

After euthanasia, 2 adjacent spinal motion segments (L4-L5 and L3-L4) were extracted from the spinal column of each of the 24 rats using a dissection microscope and surgical scalpel. Each motion segment was wrapped in plastic and then gauze soaked in PBS before being stored at −4 °C to prevent dehydration. Motion segment L4-L5 was used for μ-CT scanning to perform calcification analysis and then histologic staining and immunofluorescent labeling to assess the IVD degeneration grade and changes to chondrocyte life cycle phases. Motion segment L3-L4 was used for SEM and energy dispersive spectroscopy (EDS) imaging to examine the microstructure of CEP calcification (Figure S1D).

μ-CT and morphometric analysis

The L4-L5 motion segment was scanned using Scanco μCT40 system (Scanco Medical) at a resolution of 20 μm isotropic (45 kV × 88 uA, 340 slices). Following the scan, 3D reconstruction was performed using Amira 6.0.1 (Thermo Fisher Scientific) where bony tissue was defined as having a tissue mineral density (TMD) of 1.43 g/cm^3 as established in previous studies.[5,33,34] The bony tissue was divided into BEP and vertebral body (VB) using the growth plate, a region in the bony tissue with low TMD, and the IVD was defined as the region between the superior and inferior bony regions.

IVD calcification levels

Calcification was quantified by partitioning the IVD from the axial midplane, separating the μ-CT scan of the disc into superior and inferior regions. Using the AF-NP boarder, these regions were further delineated into central and peripheral to examine regional variability (Figures 1A, 2B). Empirical visualization and previous studies differentiated calcification from background noise and bone using a TMD threshold between 1.37 and 1.43 g/cm^3 (Figure 1E) for quantitative analysis.[5,33,34] Given the random and complex shape and spatial distribution of calcification, it was categorized into 4 phases based on size to more precisely quantify and further identify the calcification (Figure S2). Additionally, within these phases, 2 distinct calcification groups—punctate and stratified—were quantified by evaluating the number of calcification spots, the calcified volume, and the average thickness of calcification spots. The same classification method was also applied in the subsequent analysis.

BEP surface flatness

To further investigate the morphometric characteristics of the BEP, 3D reconstructions of motion segments from the central regions were meshed using Amira 6.0.1 software, ensuring uniform element size (Figure 2A). Then, based on the root-mean-square (RMS) curvature method,[35,36] the surface flatness of each node was calculated using MATLAB (Matlab2023a, MathWorks) with the following equation:

$$\kappa = \frac{1}{r},\ \kappa_{\mathrm{rms}} = \sqrt{\frac{(\kappa_{\min})^2 + (\kappa_{\max})^2}{2}},$$

where r is the radius of the circle, κ is the curvature at a point, and $\kappa_{\min}$ and $\kappa_{\max}$ are the minimum and maximum curvature at that point, respectively. The concave BEP region was selected as the region of interest (ROI) using a rectangle grid (Figure S3). Based on the surface flatness values of each node within the ROI, they are categorized into 9 levels to further analyze (Figure S4). Additionally, within these levels, 2 distinct surface flatness groups—flat and curved—were quantified by surface area and surface flatness score.

SEM and EDS analysis

SEM and EDS were employed to examine the microstructure of calcification in the CEP region. L3-L4 motion segments were submerged in optimal cutting temperature fluid (23-730-571, Thermo Fisher Scientific) on a freezing-stage microtome (SM2400, Leica Biosystems) and cut to expose the sagittal midplane. Following sectioning, samples were gently dehydrated through a series of ethanol baths (70%, 80%, 90%, 95%, and 100%) before being placed in a vacuum container for 1 wk to achieve complete dehydration. The dried samples were coated with gold using a Thin Film Gold Sputter (Dest V, Denton Vacuum) and imaged using an SEM (S-3700 N, Hitachi) and EDS (Aztec, Oxford Instruments) at magnifications of 200×, 600×, and 3 k×. Imaging conditions included an accelerating voltage of 10 kV, working distance of 10 mm, beam current of 120 μA, and resolution of 1280 × 960 pixels, with backscattered electron mode. Aztec software was used to quantify carbon, phosphorus, and calcium, generating elemental maps.

Histological staining, immunofluorescent labeling, and histopathological analysis

After μ-CT imaging was complete, the L4-L5 motion segments were fixed in 10% formalin, decalcified using 10% EDTA, then sectioned into 7 μm thick slices in the sagittal midplane plane using microtome (SM2400, Leica Biosystems). The tissue sections were then stained with H&E, following the manufacturer guidelines, and then imaged using a confocal microscope (BZ-X800, Keyence). To further examine cell life cycle, additional tissue slices obtained during sectioning were used for immunofluorescent staining. A TUNEL assay (λ_{ex} = 465 nm, λ_{em} = 515-565 nm; REF11684795910, Sigma Aldrich), staining for cell death, was performed on tissue sections following the manufacturer guidelines followed by counterstaining with DAPI (λ_{ex} = 360 nm, λ_{em} = 460 nm), which stains cell nuclei. Imaging was performed on the above-mentioned confocal microscope with a fluorescent excitation module activated and filter cubes inserted to acquire the dye emission signal.

IVD degeneration grade

Using the grading system created as a result of the ORS spine section initiative,[37] histologic analysis of the AF, NP, and endplate morphologies and NP cellularity were analyzed in each of the 4 treatment groups (n = 5-6 per group, 1 motion segment from the control cessation was damaged during preparation). Overall degeneration grade was then calculated by averaging the scores from each graded component of the IVD.

Chondrocyte life cycle phases

The chondrocyte life cycle within the inferior and superior CEP was examined by recording the number of healthy and hypertrophic cells, empty lacunae, and remodeled lacunae to produce cell ratios ([# recorded]/[healthy + hypertrophic]). Healthy and hypertrophic cells were classified based on cell morphology as described in previous literature.[38] Immunofluorescent images were processed in ImageJ (NIH, Bethesda) and quantification of TUNEL positive cells was accomplished by counting the total number of DAPI positive cells and the number of TUNEL positive cells that overlaid a DAPI positive

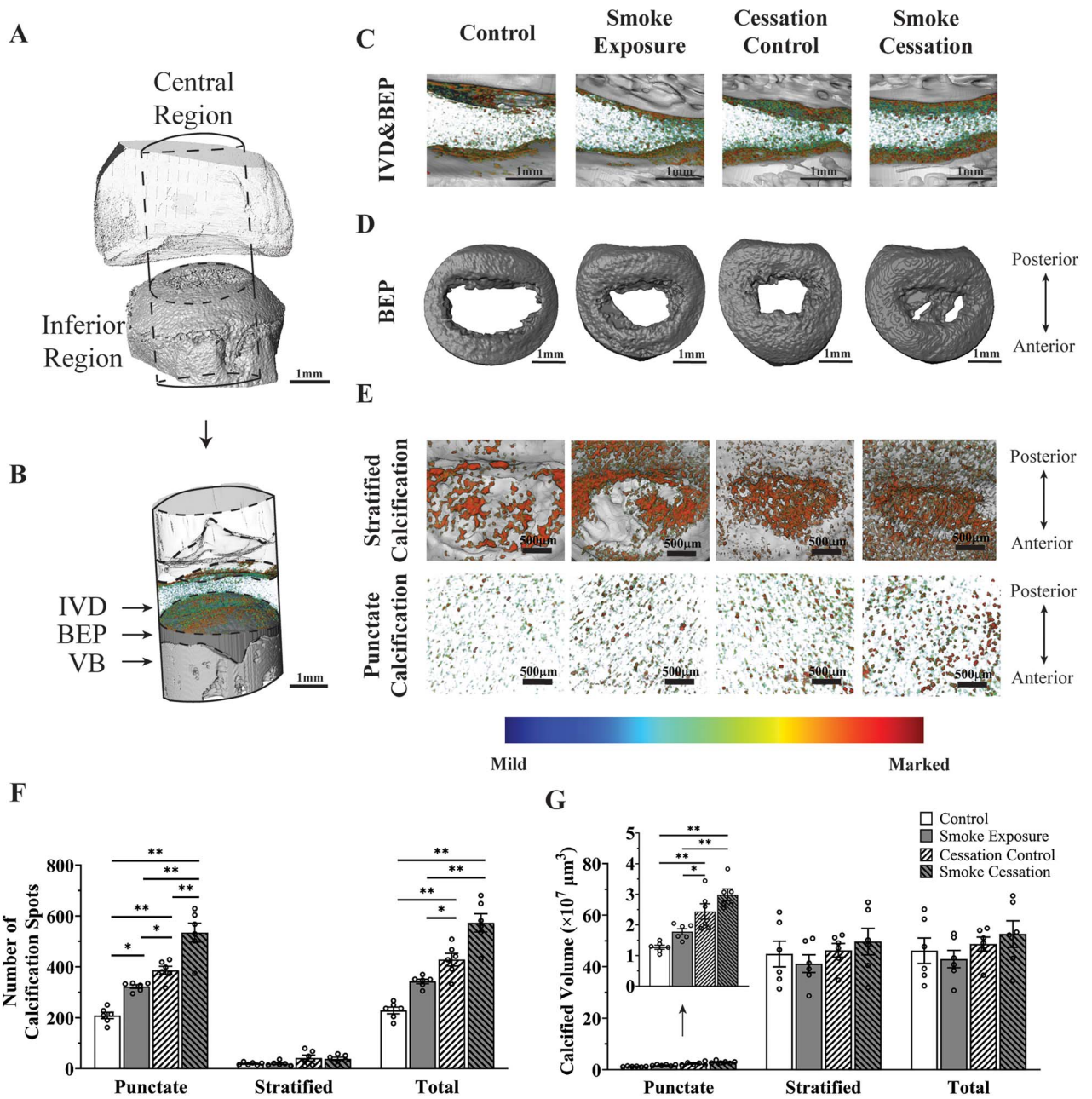

Figure 1. Effects of smoke exposure on the spatial calcification pattern of inferior central IVD region. (A) Representative 3D reconstruction of a motion segment outlining the central region of interest. (B) The division of the geometry into the IVD, BEP, and VB components. (C) Overall spatial calcification distribution in central region for each group. (D) The zoomed top-down view of BEP spatial ossification pattern. (E) The zoomed top-down view of IVD spatial calcification pattern. (F) The number of calcification spots and (G) calcified volume in IVD for the marked calcification for each group. Note: mild calcification is represented as blue to yellow and marked calcification is represented as red. Marked calcification, characterized by a TMD between 1.37 and 1.43 g/cm^3, as determined following the same method of Kague et al.[33], was selected for the quantitative calcification analysis. Specifically, calcification spots were categorized as punctate and stratified based on spot volume. Punctate calcification includes phase 1 and stratified calcification includes phase 2-4 (Figure S2). Additionally, ossified BEP was defined as having a TMD greater than 1.43 g/cm^3. * indicates p-value $< .05$, ** indicates p-value $< .001$. Data presented represent mean ± SEM. Abbreviations: BEP, bony endplate; IVD, intervertebral disc; TMD, tissue mineral density; VB, vertebral body.

cell. A TUNEL ratio (TUNEL positive cells/DAPI cells) was then created for each IVD region: anterior and posterior AF, NP, and inferior and superior CEP.

Statistical analysis

Multifactor comparative assessment

Statistics were performed using R (R Core Team, 2023). A p-value of $< .05$ was considered significant, with * indicating p-values $< .05$ and ** indicating p-values $< .001$. The Shapiro-Wilk test was used to assess the normality assumption of the data. For data following a normal distribution, 2-way and 3-way ANOVA were conducted to evaluate the effects of smoke exposure, aging, and region, as well as their interactions. This included analyses of μ-CT morphology in calcification (number, volume, and thickness of punctate and stratified calcifications), surface flatness (surface area and surface flatness score of the BEP), and chondrocyte life cycle (cell and lacunae ratios, TUNEL ratio, and cell density). Post

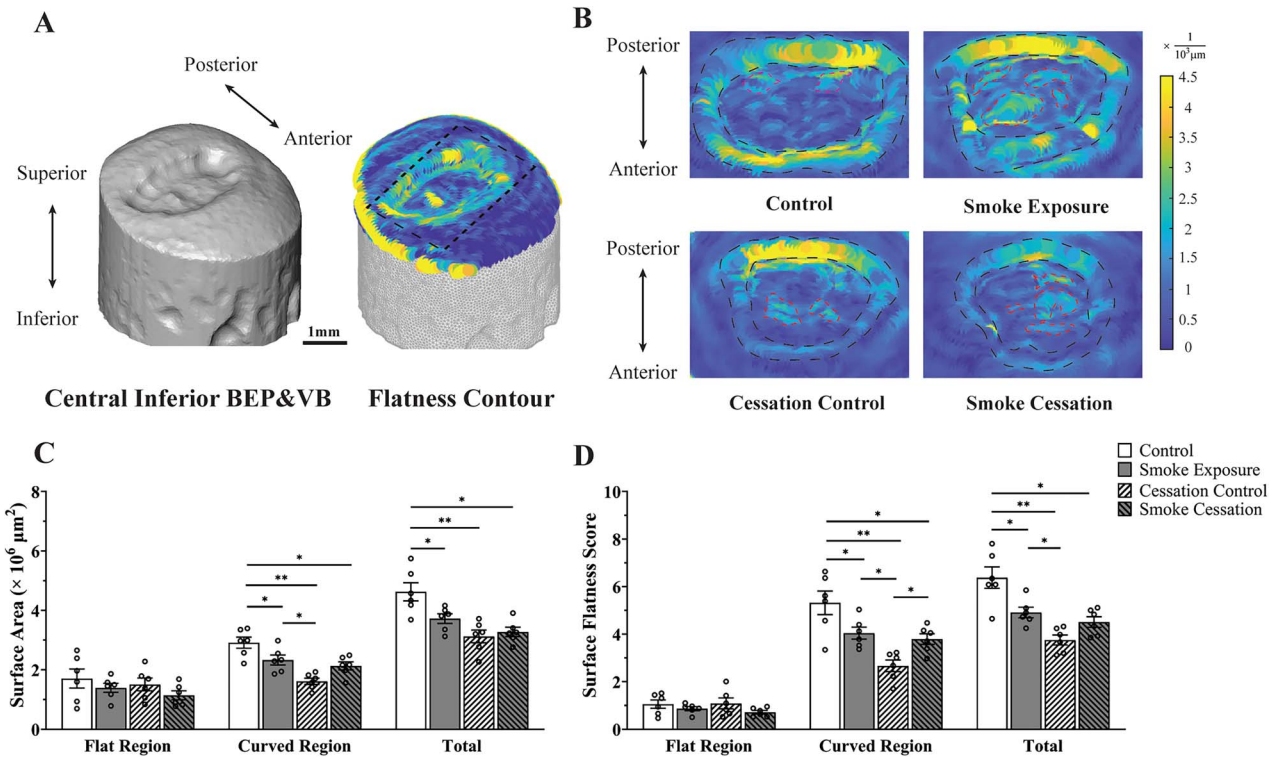

Figure 2. Effects of smoke exposure on the inferior BEP surface flatness. (A) Representative μ-CT reconstruction of the BEP and VB in the inferior central region used for curvature analysis. The dashed rectangle outlines the region of interest (ROI) (size detailed in Figure S3). (B) Representative BEP flatness analysis for each group (values of 0 indicate a perfectly flat plane). The dashed red lines highlight the aberrant calcified area. The dashed black lines annotate the edges of the concave surface of the BEP. (C) Surface area and (D) surface flatness score (flat region: level 1; curved region: levels 2-9, see Figure S4 for level breakdown) on selected ROI, for each group. * indicates p-value $< .05$, ** indicates p-value $< .001$. Data presented represent mean ± SEM. Abbreviations: BEP, bony endplate; VB, vertebral body.

hoc comparisons were conducted to further investigate the relationships between treatments and regions concerning the measured outcomes. A Holm p-value adjustment was applied to control for multiplicity error. For data not following a normal distribution, a likelihood ratio test was utilized for the 3-factor interaction analysis, followed by the Kruskal-Wallis test with Dunn's multiple comparisons test. These tests were applied to assess the IVD degeneration grade. Data in the main text are presented as mean ± SD.

PCA and correlation evaluation

All data collected using the methods described above was combined with 2D diffusion coefficients and the porosity of the AF, NP, and CEP previously measured for these specimens.[14] A PCA was performed on this combined dataset using Python, with all variables normalized prior to analysis. The elbow method was used to determine the number of principal components (PCs) to examine, based their explained variance. A bootstrap analysis ($n = 4000$) was conducted to assess the stability of the explained variance for the first 2 PCs, with resampling performed within treatment groups. The first 2 PCs of the PCA were calculated and the initial variables were ranked according to their contributions to each PC. A cluster analysis was then performed on the PCA results, with the number of clusters determined using a scree plot of the inertia. Additionally, Pearson correlation analysis was performed on the same dataset using Python, to examine the relationship between structural and diffusion properties, and between structural properties and cell life cycle.

Results

Smoke exposure increased endplate histological grade

Smoke exposure altered IVD morphology, leading to disorganization of AF lamellae, increased NP tissue hyalinization and necrosis, and endplate calcification (Figure 3A). Furthermore, histologic grading revealed that morphologic changes were dependent on smoke exposure ($p < .001$), aging ($p < .001$), and disc region ($p < .001$), with the endplate region expressing a significant deterioration under the effects (Table S1 and Figure 3B). The endplate morphology grade was higher due to smoke exposure (Control: 0.14 ± 0.21; Smoke Exposure: 0.58 ± 0.29, p=.050; Figure 3C, Table S2); however no difference was found between cessation groups (ie, cessation control vs smoke cessation). Aging resulted in a higher endplate morphology grade ($p < .05$; Figure 3C, Table S9). Additionally, smoke exposure resulted in a higher overall IVD degeneration grade (Control: 0.09 ± 0.12; Smoke Exposure: 0.34 ± 0.17, p=.045; Figure 3D, Table S2), while no difference was found between cessation groups. Aging resulted in a higher IVD degeneration grade ($p < .05$; Figure 3D and Table S1).

Smoke exposure led to aberrant CEP calcification

Punctate calcification was dependent on smoke exposure (Number: $p < .001$, Volume: $p < .001$), aging (Number: $p < .001$, Volume: $p < .001$), and CEP region (Number: $p < .001$, Volume: $p < .001$) (Table S3, Figure 1C-E). In the inferior central region, analysis of punctate calcification

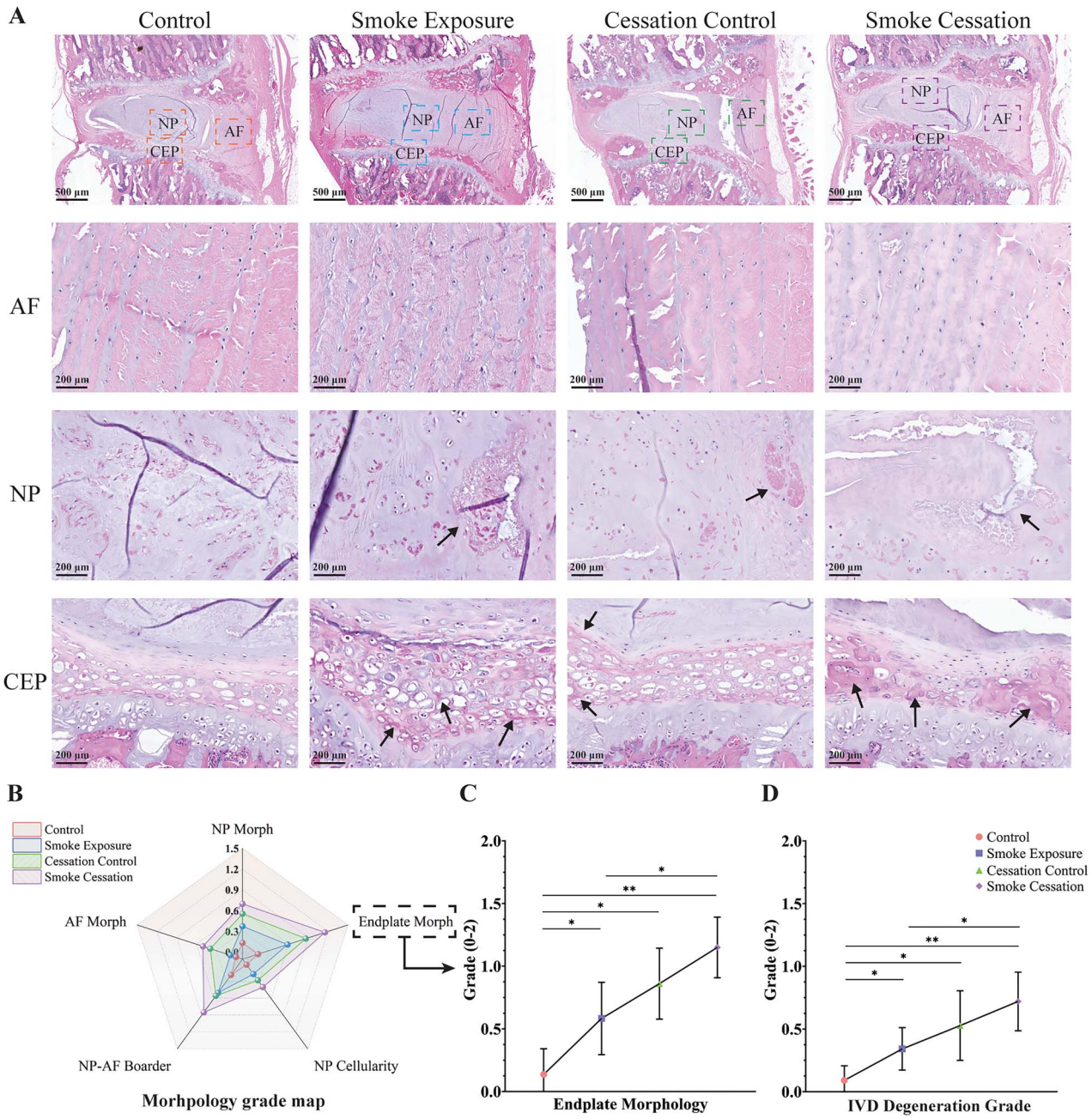

Figure 3. Effects of smoke exposure on IVD degeneration grades. (A) Representative H&E-stained sagittal sections of the IVD (AF, NP, and CEP). The black arrows indicate remodeling in the NP and calcification in the CEP. (B) Grading results illustrating the effects of smoke exposure and aging on regional histological grades (higher grade indicates a greater degree of degeneration). (C) Endplate histological grade. (D) Overall IVD degeneration grade. * indicates p-value < .05, ** indicates p-value < .001. Data presented represent mean ± SD. Abbreviations: AF, annulus fibrosis; BEP, bony endplate; CEP, cartilage endplate; IVD, intervertebral disc; NP, nucleus pulposus; VB, vertebral body.

showed higher calcification spot number due to smoke exposure (Control: 209 ± 31, Smoke Exposure: 322 ± 17, p=.003; Cessation Control: 387 ± 40, Smoke Cessation: 535 ± 91, p < .001; Figure 1F, Table S4, Video S1-4). Aging resulted in higher calcification spot number (p < .001; Figure 1F). Moreover, calcified volume did not differ due to smoke exposure (Figure 1G), while aging resulted in higher calcified volume (p < .001; Figure 1G). In the superior central region, calcification spot number was higher due to smoke exposure (p < .05; Figure S5F, Table S5). Calcified volume was higher due to smoke exposure in the cessation groups (p=.015; Figure S5G, Table S5). Aging resulted in higher calcified volume (p=.014; Figure S5G).

Analysis of stratified calcification revealed no difference in spot number or calcified volume (Figure 1F, G and Figure S5F, G). Notably, while no difference was detected for overall stratified calcification, it exhibited a unique spatial distribution, with increased calcification observed around the central region of the CEP due to smoke exposure and aging (Figure 1E and Figure S5E). SEM and EDS imaging further confirmed a similar pattern of elevated calcification in the central CEP due to exposure and aging, as suggested by the visibly larger calcification spots, higher number of spots, and denser mineral contents. (Figure 4I-L). Additionally, no difference was observed in the peripheral disc region due to smoke exposure or aging.

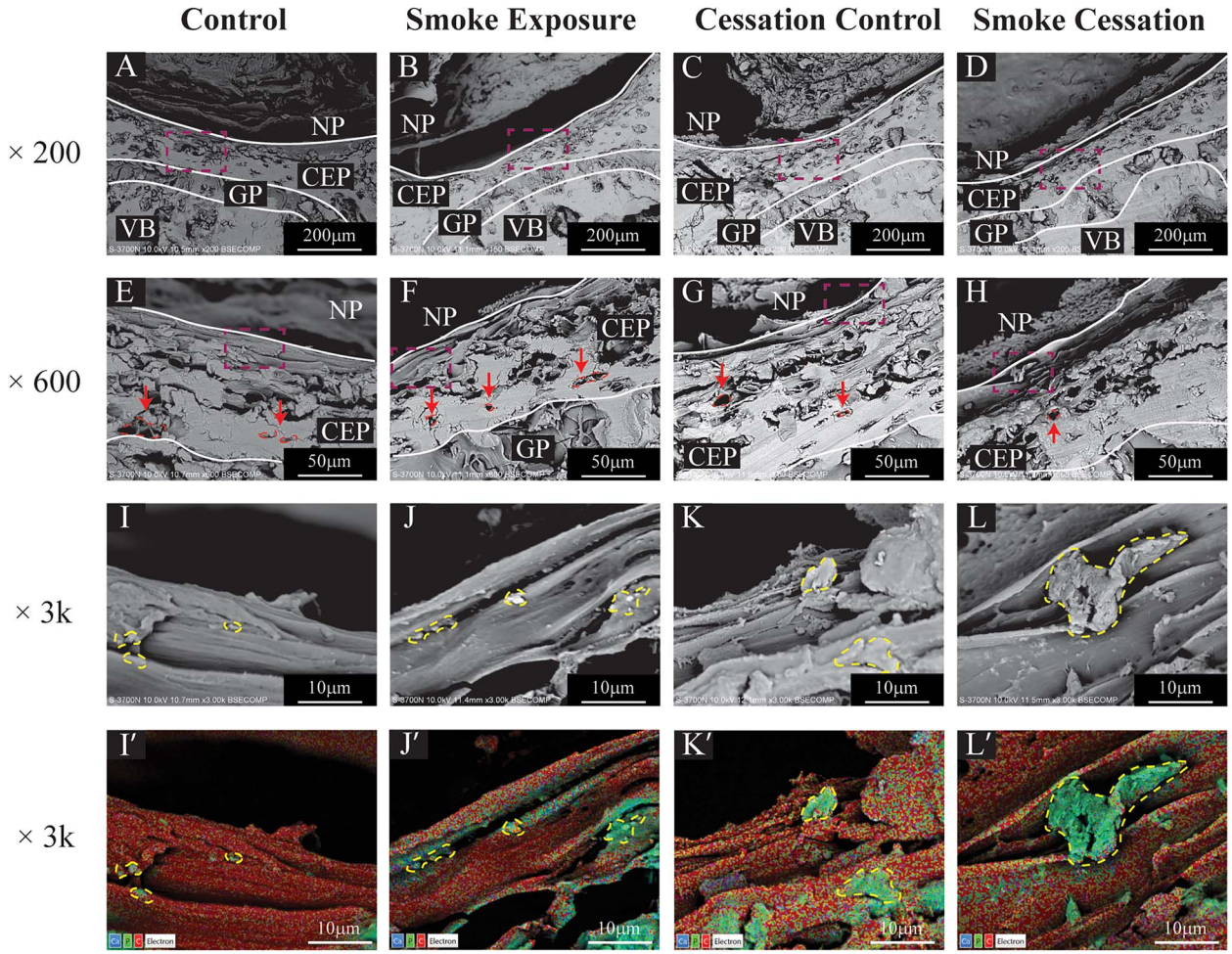

Figure 4. Representative SEM and EDS images showing calcification pattern and mineral ingredient in the inferior CEP. (A-D) SEM images of the inferior CEP. (E-H) Inferior CEP highlighting lacunae (dashed red squares) for each group. (I-L) SEM images of the punctate calcification (outlined by dashed yellow circles). (I′-L′) EDS images of the punctate calcification (outlined by dashed yellow circles). Carbon, phosphorus, and calcium are shown in red, green, and blue, respectively. Abbreviations: CEP, cartilage endplate; EDS, energy dispersive spectroscopy.

Smoke exposure altered BEP surface flatness

Surface area and flatness score were dependent on aging (Area: $p < .001$; Score: $p < .001$) and BEP region (Area: $p < .001$; Score: $p = .009$, Table S6). For the inferior BEP, surface area of the curved region was lower due to smoke exposure (Control: $(2.92 \pm 0.46) \times 10^6$ μm^2, Smoke Exposure: $(2.33 \pm 0.41) \times 10^6$ μm^2, $p = .038$; Figure 2C, Table S7); however, no difference was detected between cessation groups. Aging resulted in lower surface area ($p < .05$; Figure 2C). Moreover, the surface flatness score was lower due to smoke exposure (Control: 5.32 ± 1.21, Smoke Exposure: 4.04 ± 0.62, $p = .034$; Figure 2D, Table S7), while flatness score was higher in the smoke cessation group (Cessation Control = 2.67 ± 0.60, Smoke Cessation: 3.80 ± 0.55, $p = .046$; Figure 2D, Table S7). Aging resulted in a lower flatness score ($p < .001$; Figure 2D). The superior BEP exhibited similar trend, though no statistical significance was detected in surface area or flatness score due to smoke exposure (Figure S6C-D, Table S8); however, aging resulted in a significant decrease in surface area ($p = .038$; Figure S6C-D, Table S8).

Smoke exposure accelerated endplate chondrocyte life cycle

Histologic and immunofluorescent staining revealed that cell life cycle was dependent on smoke exposure (Remodeled lacunae: $p < .001$; TUNEL: $p < .001$), aging (Healthy cell: $p = .036$; Remodeled lacunae: $p < .001$; TUNEL: $p < .001$), and CEP region (Empty lacunae: $p = .007$; TUNEL: $p < .001$) (Tables S9 and S10). The ratio of healthy cells to total cells was lower due to smoke exposure (Control: 0.39 ± 0.11, Smoke Exposure: 0.20 ± 0.08, $p = .001$; Figure 5B, Table S11), but was higher as a result of smoke cessation (Cessation Control: 0.23 ± 0.05, Smoke Cessation: 0.42 ± 0.05, $p = .002$; Figure 5B, Table S11). In contrast, the hypertrophic cell ratio exhibited an inverse trend compared with the healthy cell ratio due to smoke exposure (Control: 0.61 ± 0.11, Smoke Exposure: $0.0.80 \pm 0.08$, $p = .001$; Cessation Control: 0.77 ± 0.05, Smoke Cessation: 0.58 ± 0.05, $p = .002$; Figure 5B, Table S11). No difference was found in empty lacunae and total lacunae ratios; however, the remodeled lacunae ratio increased due to smoke exposure (Cessation Control: 0.18 ± 0.10, Smoke Cessation: 0.65 ± 0.21, $p < .001$; Figure 5B, Table S11). Aging resulted a

similar trend with a lower healthy cell ratio ($p < .001$), higher hypertrophic cell ratio ($p < .05$), and a higher remodeled lacunae ratio ($p < .001$) (Figure 5B). In the superior CEP, no differences were observed for the healthy and hypertrophic cell ratios (Figure S7, Table S12). However, the ratio of remodeled lacunae significantly increased due to smoke exposure ($p < .001$; Figure S7, Table S12). Additionally, aging resulted in an increase in the healthy cell ratio, a decrease in the hypertrophic cell ratio, and an increase in the remodeled lacunae ratio ($p < .05$; Figure S7).

Cell death ratio was higher due to smoke exposure in the inferior CEP (Control: 0.28 ± 0.07; Smoke Exposure: 0.44 ± 0.08; p=.011; Figure 5D, Table S14), as well as NP region ($p < .05$; Figure S8). Smoke cessation resulted in a decreased cell death ratio in the inferior CEP, NP, and Anterior AF regions ($p < .05$; Figure 5D and Figure S8). Additionally, cell densities quantified from both histology and immunofluorescence imaging showed regional differences ($p < .001$; Figure S9, Table S14, and Table S15-16).

Endplate remodeling was a key indicator of IVD degeneration

The PCA showed the treatment groups to be separated along the first 2 PCs (Figure 6B) and bootstrapping analysis showed principal component 1 (PC1) and principal component 2 (PC2) to be stable (PC1: 0.295 ± 0.034; PC2: 0.190 ± 0.025, mean $\pm$ SD for $n = 4000$ bootstraps). The explained variance ratios for PC1 and PC2 were 0.26 and 0.16, respectively. Cluster analysis identified 3 distinct groups containing either the control group, smoke cessation group, or smoke exposure and cessation control group (Figure 6C). PC1 was primarily associated with CEP structural properties, including calcification, regional diffusion coefficients,[14] and histologic morphology grading (Figure 6D). PC2, on the other hand, was linked to CEP cellular parameters, such as the ratios of healthy and hypertrophic cells and empty lacunae (Figure 6E). Additionally, the correlation analysis revealed solute diffusion (obtained through FRAP studies),[14] particularly the average CEP coefficients, to be strongly correlated to CEP calcification and histologic morphology grading (Table S17). Furthermore, examination of the relationship between endplate chondrocyte life cycle and structural properties revealed the ratio of remodeled lacunae to be strongly associated with CEP calcification and morphology grading (Table S18).

Discussion

In the context of cigarette smoke exposure, IVD structural remodeling was quantified using histology, μ-CT imaging, surface flatness, and SEM/EDS analyses. Endplate remodeling (ie, aberrant cartilaginous calcification and ossification) emerged as a key indicator of cigarette smoke–induced IVD degeneration. First, histological analysis of the smoke exposure group displayed an increased staining intensity in the CEP, more characteristic of mineralized bony tissue. Histological analysis also confirmed the presence of IVD degeneration by revealing AF collagen fiber bundle disorganization and increased NP hyalinization and fibrosis in the smoke exposure group, consistent with observations from previous studies.[13,15,16] When further grading IVD degeneration using a standardized scoring system,[37] the analysis showed that smoke exposure led to a pronounced increase in the degeneration score, particularly in the CEP. Secondly, surface flatness analysis of the BEP surface, used to characterize the ossified CEP, showed an increase in the flatness score of the BEP-CEP interface following smoke exposure. This finding indicated the growth of the BEP in the central concave region due to the progressive ossification of the CEP. Lastly, SEM/EDS imaging confirmed irregular calcium phosphorus deposits and mineralization pattern in the endplate region, consistent with the findings from histological, and surface flatness analyses, all as a result of smoke exposure. Interestingly, the inferior endplate seems slightly more sensitive to remodeling due to smoke exposure, possibly due to asymmetric endplate anatomy and the stage of endplate maturation.

To further explore the potential mechanisms of endplate remodeling at the cellular level, the life cycle of CEP chondrocytes was characterized using histological and immunohistochemical analyses. Cigarette smoke exposure appeared to accelerate the cell life cycle, driving chondrocytes more rapidly into the apoptotic phase, as evidenced by a reduction in healthy chondrocytes, an increase in hypertrophic and TUNEL positive cells. This progression correlated with the observed endplate calcification and ossification. A slight trend of increased empty lacunae was also noted. In line with findings in other orthopedic conditions like osteoarthritis, chondrocyte hypertrophy, often a precursor to terminal differentiation, is associated with increased expression of matrix-degrading enzymes and collagen type X, promoting extracellular matrix calcification.[39,40] Smoke exposure likely exacerbates these effects through oxidative stress driven by ROS, leading to DNA damage, mitochondrial dysfunction, and apoptosis.[41] This oxidative stress may also result from nutrient deprivation caused by the recession of subchondral vascular buds, a consequence of smoking.[15,42] These combined factors could contribute to the accelerated chondrocyte life cycle, aberrant endplate calcification, and degenerative IVD remodeling. Future research is needed to further elucidate the relationship between oxidative stress and cellular injury in the context of cigarette smoke exposure.

In recent years, the number of current smokers has steadily decreased (from approximately 32.7% to 21.7%),[1] leading to an increase in patients undergoing smoking cessation. However, the effects of smoking cessation on IVD degeneration remain largely unexplored. This study demonstrated that endplate pathological remodeling progressively deteriorates, suggesting that smoking cessation alone cannot reverse endplate mineralization process. Specifically, histologic grading of the CEP region tended to worsen in the smoke cessation group. Moreover, both the number and volume of calcification spots increased significantly, indicating that remodeling of the CEP persisted even after smoke exposure ended. Surface flatness analysis further showed that localized flatness decreased in the central disc region. These results suggested that the CEP and BEP remodeling continued even after smoke exposure has ceased. Interestingly, while the cell life cycle in the smoke cessation group returned to levels like those in the control group, however, the number of remodeled lacunae in CEP was much higher than in any other groups. This suggested that remodeling still occurs at the cellular level despite the ratio of healthy to hypertrophic chondrocytes returning to normal. This conclusion is supported by 2 previous studies, which found that the remodeling of AF collagen fiber bundles appears to be irreversible,[16] and a tendency of CEP calcification.[14]

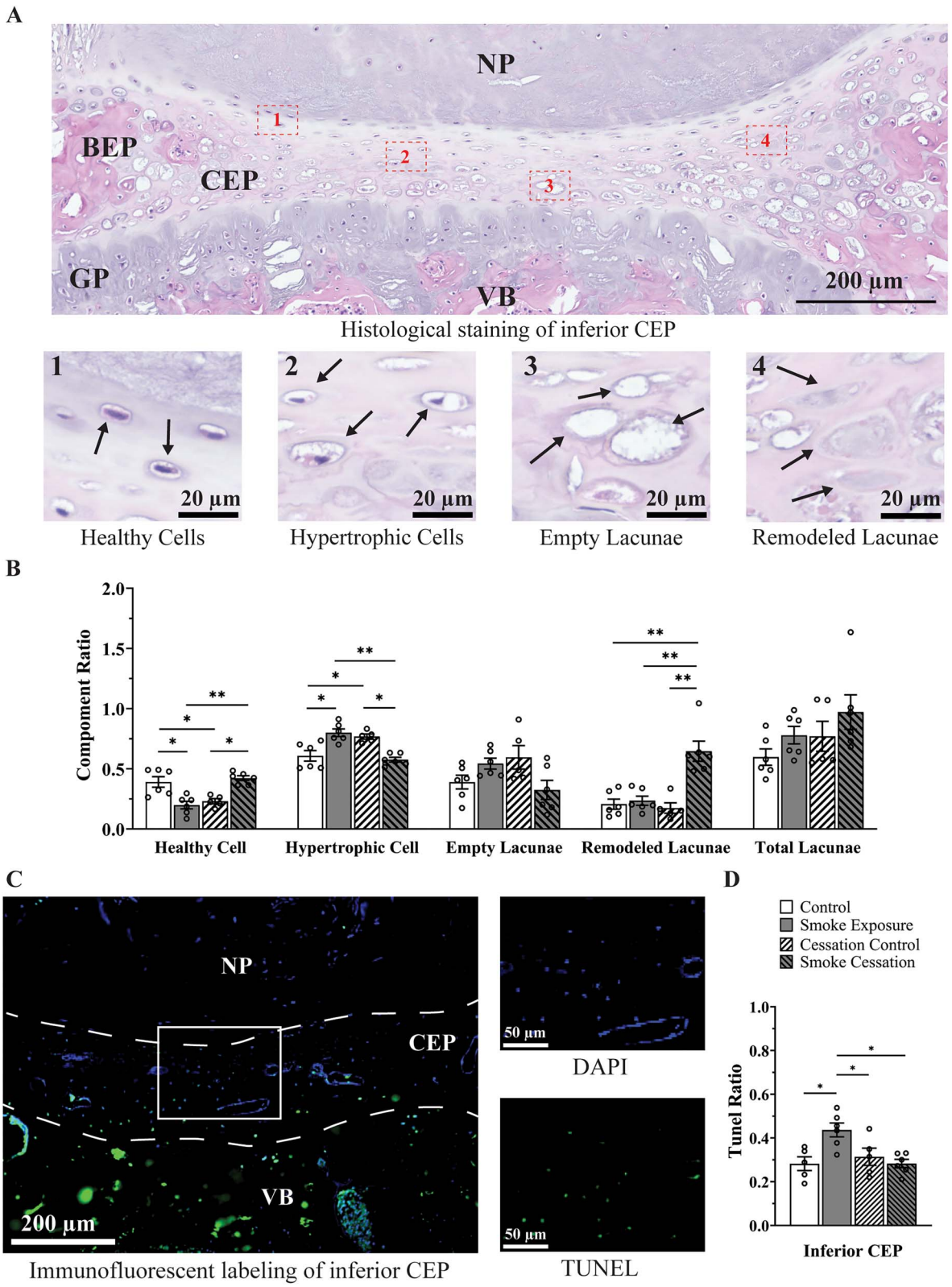

Figure 5. Effect of smoke exposure on inferior CEP cell life cycle. (A) Representative CEP region and corresponding cell types analyzed by H&E staining. (B) Cell ratios for each cell type counted (healthy cell, hypertrophic cell, empty lacunae, remodeled lacunae, and total lacunae) were calculated for each group. (C) Representative immunofluorescent CEP image with DAPI and TUNEL channels shown for the boxed region. (D) TUNEL ratio of the inferior CEP. * indicates p-value < .05, ** indicates p-value < .001. Data presented represent mean ± SEM. Abbreviation: CEP, cartilage endplate.

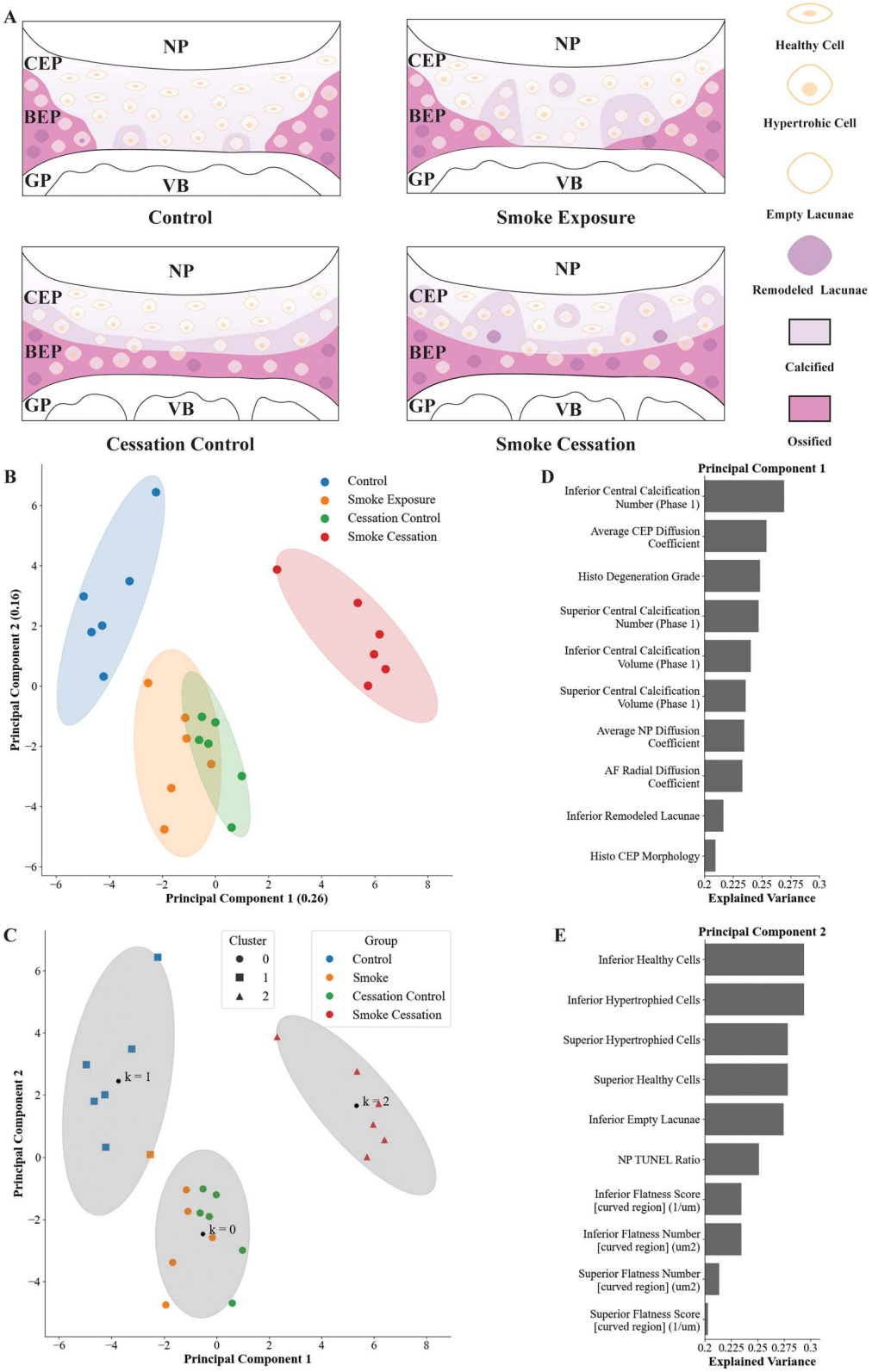

Figure 6. (A) Schematic figure illustrating the association between calcification patterns and cell life cycle alterations during the IVD degeneration process for each group. (B) Scatterplot of each specimen on the first 2 principal components with 95% confidence ellipses for each treatment group. (C) Scatterplot of the cluster analysis ($k = 3$) where marker shape and color represent the cluster and treatment group each marker belongs to, respectively. Gray 95% confidence ellipses represent each cluster. The top 10 variables for (D) PC1 and (E) PC2 which had the most influence on their respective explained variance. Abbreviations: IVD, intervertebral disc; PC1, principal component 1; PC2, principal component 2.

The thoracic region of the spinal column of the same rats was analyzed in our previous study for solute diffusion properties,[14] which are crucial for understanding how the 3-dimensional structure and composition impact the integrity of avascular IVD tissues, thereby defining their biomechanical function.[43] To identify the most influential factors in this animal model, a PCA was conducted, which analyzed morphological and solute diffusion properties,[14] and identified the endplate as the most sensitive component to calcification remodeling in the context of cigarette smoke exposure (Figure 6D and E). This was evidenced by 2 key findings: first, PC1 emphasized tissue-level remodeling of the endplate, with factors related to CEP structure and solute diffusion properties being the top contributors; second, PC2 highlighted cellular-level alterations, particularly in the chondrocyte life cycle, with notable changes in the balance of healthy and hypertrophic cells (Figure 6E). The cluster analysis performed Correlation analysis further reinforced these findings, revealing a statistically significant positive relationship between cellular changes—such as remodeled lacunae in endplate regions—and tissue-level changes, including calcification number, volume, and CEP morphologic grade, effectively linking cellular disruption to tissue-level remodeling (Table S3). Additionally, it should be noted that morphological features, cell life cycle characterizations, and calcification patterns were sampled only from the endplate, introducing some bias in the PCA toward this region compared with NP or AF.

Interestingly, a moderate difference in endplate remodeling patterns was observed between smoke exposure and aging. Smoke exposure led to aberrant calcification concentrated more in the central concave region, while aging followed a pattern of peripheral calcification that gradually migrated and fused into the central endplate region (Figures 4E-H, 2B and Figure S6B, S10E-H). This aging pattern is reminiscent of the endplate maturation process seen in postnatal development, where ossification begins in the periphery and progresses inward,[44,45] further illustrating the distinct impacts of smoke exposure and aging on endplate remodeling.

Earlier nicotine pump models maintain controlled nicotine levels in the blood over extended periods but fail to account for the additional toxic chemicals in cigarette smoke that may influence IVD pathophysiology.[13,15] Second-hand smoke exposure models offer a more physiologically relevant approach by exposing animals to smoke,[16,30,46] yet they omit the direct effects of first-hand smoke inhalation. Our model differs by using a custom smoke exposure apparatus to expose the animals to both first-hand smoke, drawn directly through the cigarette butts, and second-hand smoke, pumped from the air surrounding a burning cigarette. This approach was designed to produce a more systemic and physiological impact on the IVD. Moreover, SD rats were selected for this study because their CEP to disc ratio (10%-25%; human ~11.3%) is significantly larger than that of other animals, such as bovine (~5.3%) or rabbit (~1%),[47,48] making them particularly suited for studying CEP calcification and ossification. This characteristic, combined with their faster aging cycle,[31] enhances the efficiency and relevance of the model for examining endplate remodeling throughout the IVD degeneration process. Notably, to our knowledge, this is the first study to demonstrate the 3-dimensional BEP morphology in rat IVD and to quantify the endplate remodeling process during aging in the context of cigarette smoke exposure. The capacity for gene knockouts in rodents further enhances their suitability as animal models for investigating the biological pathways and potential therapeutic targets involved in endplate remodeling during IVD degeneration. This model offers flexibility in studying endplate remodeling under various smoking conditions, as the smoke exposure dosage can be easily modified by adjusting TPM levels or exposure duration to simulate different scenarios (eg, acute vs chronic; light vs heavy smoking).

Like all models, this one has its limitations. First, rats have a much faster metabolism than humans and other larger animals, causing them to process cigarette constituents more rapidly, which could affect the comparability of results to larger animal models.[31] Additionally, while the ratio of endplate to disc in the rat IVD is closer to that of humans than in porcine or rabbit models, the actual size of the rat IVD is much smaller, requiring caution when extrapolating findings related to the role of the endplate in nutrient supply to the IVD.[49] This model also cannot differentiate which specific factors—such as smoke exposure, blood supply, nutrient environment, or cigarette constituents—play the dominant role in IVD remodeling due to the accumulated systemic effects of cigarette smoke exposure.

There are also methodological limitations in this study. Histologic analysis did not differentiate cell types within the various regions of the IVD and endplate for the cell density measurements. Additionally, the random and complex shape and spatial distribution of calcification spots, combined with the μ-CT resolution, posed challenges in distinguishing background noise and obtaining precise quantification. To address these challenges, a classification approach based on CEP calcification spot size (punctate vs stratified) and BEP surface nodal flatness (flat vs curved) was employed. This method helped identify which partition types were most sensitive to smoke exposure and determine appropriate cutoff points for more precise analysis. The chondrocyte death trend observed following smoke exposure in this study was similar to that reported by Nakahashi et al.,[46] though not as pronounced, likely due to the use of younger, skeletally immature animals in that study. Another limitation is the relatively small, all male sample size utilized for this study. A small sample size constrained the statistical power of this study and prevented examination of the effect of smoke exposure at the molecular level. Experiments at the molecular level were neglected as the aim of this study was to examine how structural remodeling occurred as a result of smoke exposure and cessation. Additionally, while performing this study with both male and female rats would have enhanced the generalizability of the study, only males were utilized to reduce the effect of sex and focus only on the effect of smoke exposure on the specimens. The sample size also affected the PCA leading to instability of the component loadings that contribute to each PC. While the PCs are stable as demonstrated by the bootstrapping analysis, unstable loadings hinder the generalizability of the PCA. Although this analysis serves as an exploratory tool, future investigations will incorporate larger scale animal experiments to provide more comprehensive and generalizable insights. Along with expanding sample size, subsequent studies will aim to investigate the molecular mechanisms underlying the impact of smoke exposure, with a particular focus on gene expression and protein analysis, to provide a deeper understanding of how smoke exposure drives calcification processes and what causes smoke exposure–induced IVD

degeneration. Finally, it is essential to note that all the rats in this study were initially part of a femoral fracture healing study where both femurs of all rats were broken to examine the effect of smoke exposure on different healing methods.[5] This could potentially influence the baseline physiology of the IVD. However, since all animals underwent femoral fracture healing, the baseline conditions should generally be consistent across the groups, allowing for a valid comparison of the effects of smoke exposure and smoke cessation on endplate remodeling during IVD degeneration.

In conclusion, endplate remodeling, marked by aberrant cartilaginous calcification and ossification, and driven by an accelerated chondrocyte cell life cycle that potentially pushes chondrocytes more rapidly into the apoptotic phase, emerged as a key indicator of cigarette smoke–induced IVD degeneration. Importantly, smoking cessation alone was insufficient to reverse the mineralization progression in the endplate, highlighting the persistent impact of smoke exposure history during the aging process. Principal component analysis further confirmed the endplate's susceptibility to remodeling under cigarette smoke exposure, with tissue-level changes in CEP structure and solute diffusion properties, and cellular-level alterations in the chondrocyte life cycle identified as the most significant contributors. These findings underscore the significance of endplate remodeling in IVD degeneration and its promising potential as a target for future mechanistic studies and therapeutic interventions to improve disc health.

Acknowledgments

We would like to thank Dr. Vincent D. Pellegrini, Jr. and Dr. Russell A. Reeves for their support on the development of the custom smoke exposure room and smoke exposure protocol. We would also like to thank Karly Ripple for assisting with histological and immunofluorescent analyses.

Author contributions

Joshua Kelley and Hui Li contributed equally to this work. Joshua Kelley (Data curation, Formal analysis, Investigation, Methodology, Project Administration, Writing—original draft, review & editing), Hui Li (Data curation, Formal analysis, Investigation, Methodology, Writing—original draft, review & editing), Yi Sun (Methodology, Software), Pengling Ren (Methodology, Software), Guanghua Chen (Methodology, Software), Shuchun Sun (Methodology, Software), Jichao Zhao (Methodology, Software), Nathan Buchweitz (Formal analysis, Investigation, Software, Visualization, Writing—review & editing), Michael Kern (Conceptualization, Methodology, Writing—review & editing), Charles A. Reitman (Conceptualization, Methodology, Writing—review & editing), Danyelle M. Townsend (Writing—review & editing), Hai Yao (Conceptualization, Funding acquisition, Resources, Supervision), and Yongren Wu (Conceptualization, Data curation, Formal analysis, Funding acquisition, Project Administration, Resources, Supervision, Writing—review & editing)

Supplementary material

Supplementary material is available at *JBMR Plus* online.

Funding

Financial support was received from the National Institute of Health Grants P20GM121342 and R01DE021134, and the Seed Starter Grant awarded by the Cervical Spine Research Society.

Conflicts of interest

The authors have no conflicts of interest to be disclosed.

Data availability

Data analyzed and presented in this study are available from the corresponding author upon sensible request.

References

1. Commar A, Prasad V, D'Espaignet ET. *WHO Global Report on Trends in Prevalence of Tobacco Use 2000-2030*. World Health Organization; 2024:135.
2. Barnes PJ, Burney PGJ, Silverman EK, et al. Chronic obstructive pulmonary disease. *Nat Rev Dis Primers*. 2015;1:1-21. https://doi.org/10.1038/nrdp.2015.76
3. US Department of Health and Human Services. *The Health Consequences of Smoking—50 Years of Progress: A Report of the Surgeon General*. U.S. Department of Health and Human Services, Public Health Service, Office on Smoking and Health; 2014. Accessed June 19, 2024. https://doi.org/10.1037/e510072014-001
4. Sloan A, Hussain I, Maqsood M, Eremin O, El-Sheemy M. The effects of smoking on fracture healing. *Surgeon*. 2010;8:111-116. https://doi.org/10.1016/j.surge.2009.10.014
5. Reeves R, Wu Y, Hanna EL, et al. Cigarette smoke exposure impairs fracture healing in a rat model: preferential impairment of endochondral over membranous healing. *J Biomech Eng* Published online October. 2024;147:1-40. https://doi.org/10.1115/1.4066796
6. Battie M, Videman T, Gill K, et al. Smoking and lumbar intervertebral disc degeneration: an MRI study of identical twins. *Spine*. 1991;16:1015-1021. https://doi.org/10.1097/00007632-199109000-00001
7. Leboeuf-Yde C, Kjær P, Bendix T, Manniche C. Self-reported hard physical work combined with heavy smoking or overweight may result in so-called Modic changes. *BMC Musculoskelet Disord*. 2008;9:5. https://doi.org/10.1186/1471-2474-9-5
8. Malham GM, Johnson N, Claydon MH. Modic changes on magnetic resonance imaging and smoking history predict vascular adherence during anterior lumbar exposure. *Int J Spine Surg*. 2021;15:1054-1059. https://doi.org/10.14444/8190
9. Rajesh N, Moudgil-Joshi J, Kaliaperumal C. Smoking and degenerative spinal disease: a systematic review. *Brain and Spine*. 2022;2:100916. https://doi.org/10.1016/j.bas.2022.100916
10. Chen Z, Li X, Pan F, Wu D, Li H. A retrospective study: does cigarette smoking induce cervical disc degeneration? *Int J Surg*. 2018;53:269-273. https://doi.org/10.1016/j.ijsu.2018.04.004
11. Akmal M, Kesani A, Anand B, Singh A, Wiseman M, Goodship A. Effect of nicotine on spinal disc cells: a cellular mechanism for disc degeneration. *Spine*. 2004;29:568-575. https://doi.org/10.1097/01.BRS.0000101422.36419.D8
12. Vo N, Wang D, Sowa G, et al. Differential effects of nicotine and tobacco smoke condensate on human annulus fibrosus cell metabolism. *J Orthop Res*. 2011;29:1585-1591. https://doi.org/10.1002/jor.21417
13. Uematsu Y, Matuzaki H, Iwahashi M. Effects of nicotine on the intervertebral disc: an experimental study in rabbits. *J Orthop Sci*. 2001;6:177-182. https://doi.org/10.1007/s007760100067
14. Kelley J, Buchweitz N, Madden A, et al. Effect of cigarette smoke exposure and cessation on regional diffusion properties in rat intervertebral discs. *JOR Spine*. 2024;7:e70015. https://doi.org/10.1002/jsp2.70015
15. Iwahashi M, Matsuzaki H, Tokuhashi Y, Wakabayashi K, Uematsu Y. Mechanism of intervertebral disc degeneration caused by nicotine in rabbits to explicate intervertebral disc disorders caused by smoking. *Spine*. 2002;27:1396-1401. https://doi.org/10.1097/00007632-200207010-00005

16. Nemoto Y, Matsuzaki H, Tokuhasi Y, et al. Histological changes in intervertebral discs after smoking cessation: experimental study using a rat passive smoking model. *J Orthop Sci*. 2006;11:191-197. https://doi.org/10.1007/s00776-005-0987-4
17. Wu Y, Cisewski SE, Wegner N, et al. Region and strain-dependent diffusivities of glucose and lactate in healthy human cartilage endplate. *J Biomech*. 2016;49:2756-2762. https://doi.org/10.1016/j.jbiomech.2016.06.008
18. Buchweitz N, Sun Y, Cisewski Porto S, et al. Regional structure-function relationships of lumbar cartilage endplates. *J Biomech*. 2024;169:112131. https://doi.org/10.1016/j.jbiomech.2024.112131
19. Berg-Johansen B, Fields AJ, Liebenberg EC, Li A, Lotz JC. Structure-function relationships at the human spinal disc-vertebra interface: structure-function of the disc-vertebra Interface. *J Orthop Res*Published online June. 2017;36:192-201. https://doi.org/10.1002/jor.23627
20. DeLucca JF, Cortes DH, Jacobs NT, Vresilovic EJ, Duncan RL, Elliott DM. Human cartilage endplate permeability varies with degeneration and intervertebral disc site. *J Biomech*. 2016;49:550-557. https://doi.org/10.1016/j.jbiomech.2016.01.007
21. Cortes DH, Jacobs NT, DeLucca JF, Elliott DM. Elastic, permeability and swelling properties of human intervertebral disc tissues: a benchmark for tissue engineering. *J Biomech*. 2014;47:2088-2094. https://doi.org/10.1016/j.jbiomech.2013.12.021
22. Wu Y, Cisewski SE, Sun Y, et al. Quantifying baseline fixed charge density in healthy human cartilage endplate: a two-point electrical conductivity method. *Spine*. 2017;42:E1002-E1009. https://doi.org/10.1097/BRS.0000000000002061
23. Wu Y, Cisewski S, Sachs BL, Yao H. Effect of cartilage endplate on cell based disc regeneration: a finite element analysis. *Mol Cell Biomech*. 2013;10:159-182.
24. Urban JP, Roberts S. Degeneration of the intervertebral disc. *Arthritis Res Ther*. 2003;5:120-130. https://doi.org/10.1186/ar629
25. Adams MA, Roughley PJ. What is intervertebral disc degeneration, and what causes it? *Spine*. 2006;31:2151-2161. https://doi.org/10.1097/01.brs.0000231761.73859.2c
26. Lotz JC, Fields AJ, Liebenberg EC. The role of the vertebral end plate in low back pain. *Global Spine J*. 2013;3:153-163. https://doi.org/10.1055/s-0033-1347298
27. Fields AJ, Liebenberg EC, Lotz JC. Innervation of pathologies in the lumbar vertebral endplate and intervertebral disc. *Spine J*. 2014;14:513-521. https://doi.org/10.1016/j.spinee.2013.06.075
28. Urban J, Roberts S. Development and degeneration of the intervertebral discs. *Mol Med Today*. 1995;1:329-335. https://doi.org/10.1016/S1357-4310(95)80032-8
29. Ferguson SJ, Steffen T. Biomechanics of the aging spine. *Eur Spine J*. 2003;12:S97-S103. https://doi.org/10.1007/s00586-003-0621-0
30. Numaguchi S, Esumi M, Sakamoto M, et al. Passive cigarette smoking changes the circadian rhythm of clock genes in rat intervertebral discs. *J Orthop Res*. 2016;34:39-47. https://doi.org/10.1002/jor.22941
31. Agoston DV. How to translate time? The temporal aspect of human and rodent biology. *Front Neurol*. 2017;8:92. https://doi.org/10.3389/fneur.2017.00092
32. Sengupta P. The laboratory rat: relating its age with human's. *Int J Prev Med*. 2013;4:624-630.
33. Kague E, Turci F, Newman E, et al. 3D assessment of intervertebral disc degeneration in zebrafish identifies changes in bone density that prime disc disease. *Bone Res*. 2021;9:39-16. https://doi.org/10.1038/s41413-021-00156-y
34. Farooq S, Leussink S, Sparrow LM, et al. Cortical and trabecular morphology is altered in the limb bones of mice artificially selected for faster skeletal growth. *Sci Rep*. 2017;7:10527. https://doi.org/10.1038/s41598-017-10317-x
35. Ateshian GA, Rosenwasser MP, Mow VC. Curvature characteristics and congruence of the thumb carpometacarpal joint: differences between female and male joints. *J Biomech*. 1992;25:591-607. https://doi.org/10.1016/0021-9290(92)90102-7
36. Lenz AL, Krähenbühl N, Peterson AC, et al. Statistical shape modeling of the talocrural joint using a hybrid multi-articulation joint approach. *Sci Rep*. 2021;11:7314. https://doi.org/10.1038/s41598-021-86567-7
37. Lai A, Gansau J, Gullbrand SE, et al. Development of a standardized histopathology scoring system for intervertebral disc degeneration in rat models: an initiative of the ORS spine section. *JOR Spine*. 2021;4:e1150. https://doi.org/10.1002/jsp2.1150
38. Rogers AW, Cisewski SE, Kern CB. The zonal architecture of the mandibular condyle requires ADAMTS5. *J Dent Res*. 2018;97:1383-1390. https://doi.org/10.1177/0022034518777751
39. Rim YA, Nam Y, Ju JH. The role of chondrocyte hypertrophy and senescence in osteoarthritis initiation and progression. *Int J Mol Sci*. 2020;21:2358. https://doi.org/10.3390/ijms21072358
40. van der Kraan PM, van den Berg WB. Chondrocyte hypertrophy and osteoarthritis: role in initiation and progression of cartilage degeneration? *Osteoarthr Cartil*. 2012;20:223-232. https://doi.org/10.1016/j.joca.2011.12.003
41. Caliri AW, Tommasi S, Besaratinia A. Relationships among smoking, oxidative stress, inflammation, macromolecular damage, and cancer. *Mutat Res Rev Mutat Res*. 2021;787:108365-105742. https://doi.org/10.1016/j.mrrev.2021.108365
42. Holm S, Nachemson A. Nutrition of the intervertebral disc: acute effects of cigarette smoking: an experimental animal study. *Ups J Med Sci*. 1988;93:91-99. https://doi.org/10.1517/03009734000000042
43. Chen P, Chen X, Hepfer RG, et al. A noninvasive fluorescence imaging-based platform measures 3D anisotropic extracellular diffusion. *Nat Commun*. 2021;12:1913. https://doi.org/10.1038/s41467-021-22221-0
44. Wang F, Zhang C, Sinkemani A, et al. A histocytological and radiological overview of the natural history of intervertebral disk: from embryonic formation to age-related degeneration. *Eur Spine J*. 2019;28:633-648. https://doi.org/10.1007/s00586-019-05903-8
45. Crump KB, Alminnawi A, Bermudez-Lekerika P, et al. Cartilaginous endplates: a comprehensive review on a neglected structure in intervertebral disc research. *JOR Spine*. 2023;6:e1294. https://doi.org/10.1002/jsp2.1294
46. Nakahashi M, Esumi M, Tokuhashi Y. Detection of apoptosis and matrical degeneration within the intervertebral discs of rats due to passive cigarette smoking. *PLoS One*. 2019;14:e0218298. https://doi.org/10.1371/journal.pone.0218298
47. Seol D, Choe H, Ramakrishnan PS, et al. Organ culture stability of the intervertebral disc: rat versus rabbit. *J Orthop Res*. 2013;31:838-846. https://doi.org/10.1002/jor.22285
48. Lakstins K, Arnold L, Gunsch G, Khan S, Moore S, Purmessur D. Characterization of bovine and canine animal model cartilage endplates and comparison to human cartilage endplate structure, matrix composition, and cell phenotype. *JOR Spine*. 2020;3:e1116. https://doi.org/10.1002/jsp2.1116
49. Li Y, Wu H, Li Z, et al. Species variation in the cartilaginous endplate of the lumbar intervertebral disc. *JOR Spine*. 2022;5:e1218. https://doi.org/10.1002/jsp2.1218

JBMR Plus, 2025, 9, ziaf016
https://doi.org/10.1093/jbmrpl/ziaf016
Research Article